INTERNATIONAL JOURNAL OF PRECISION ENGINEERING AND MANUFACTURING Vol. 16, No. 7, pp. 1609-1615 JUNE 2015 / 1609
DOI: 10.1007/s12541-015-0211-1 ISSN 2234-7593 (Print) / ISSN 2005-4602 (Online)

Analytic Approaches for Keeping High Braking Efficiency and Clamping Efficiency of Electro Wedge Brakes

Dong-Hwan Shin[1,2,#], Seonghun Lee[1], Choong-Pyo Jeong[1,2], Oh-Seok Kwon[3], Tae-Sang Park[1], Sung-Ho Jin[1], Dong Hoon Ban[1], and Seung-Han Yang[2]

1 DGIST Convergence Research Center for Future Automotive Technology, 333, Techno jungang-daero, Hyeonpung-myeon, Dalseong-gun, Daegu, 711-873, South Korea
2 Department of Mechanical Engineering, Kyungpook National University, 80, Daehak-ro, Buk-gu, Daegu, 702-701, South Korea
3 DGIST Convergence Research Center for Wellness, 333, Techno jungang-daero, Hyeonpung-myeon, Dalseong-gun, Daegu, 711-873, South Korea
Corresponding Author / E-mail: sdh77@dgist.ac.kr, TEL: +82-53-785-4621, FAX: +82-53-785-4479

KEYWORDS: Electro wedge brake, Electro mechanical brake, Clamping force, Self-reinforcing effect, Variable wedge structure, Estimation of frictional coefficient

The transfer from engine drive vehicles to electric vehicle has been proceeding due to fuel exhaustion, higher fuel costs, and environmental restrictions. This trend has also led to a transition in brake system from the hydraulic brake system to the electric brake system, which uses electric power. This electric brake system has led to an enhancement of safety and eco-friendliness due to a reduction braking distance, a rapid-response property, and the elimination of braking oil. However, one of the big problems to solve for practical usages is the need of a high power motor to enable braking forces as strong as those of hydraulic brake systems. Therefore, it is necessary to develop high efficiency electro mechanical brakes with a proper reinforcement mechanism to solve this problem. In this paper, we describe a wedge structure that has a self-reinforcing effect; we propose a proper actuating direction for a movable wedge to obtain greater clamping efficiency and braking efficiency, which will mean a better relation of the motor force as the input to the braking force as the output. Further, we propose the method to keep the most braking efficiency and clamping efficiency without reference to the variations of frictional coefficient.

Manuscript received: July 16, 2014 / Revised: February 26, 2015 / Accepted: May 10, 2015

NOMENCLATURE

F_b = braking force
F_m = actuating force
F_n = clamping force
μ = frictional coefficient
α = wedge inclinational angle
β = actuating angle
C_b* = braking efficiency (F_b / F_m)
C_n*= clamping efficiency (F_n / F_m)

1. Introduction

Calipers are used for the deceleration and stopping of braking targets such as discs in vehicles. Hydraulic power has been used as the energy source for conventional hydraulic calipers. Existing hydraulic braking systems in vehicles are composed of the brake pedal, the hydraulic booster, and the hydraulic caliper. The driver transmits braking intent through the brake pedal stroke and force. The hydraulic booster can amplify the pedal force only when the engine operates. The hydraulic caliper is composed of cylinders and pistons. There are also hydraulic pipes from the booster to the caliper. Currently, X-by-wire technology is actively being studied because of the decreasing supply of fossil fuels and strict CO_2 regulations.

As part of this trend, the e-pedal and the electro mechanical brake (EMB) are also being investigated. This EMB is anticipated to be the next generation of brake systems because future vehicles will use electric batteries and not engines. Furthermore, the EMB is also adequate for the low speed driving of transitional hybrid vehicles. On the other hand, this EMB has a better response time than that of conventional hydraulic brake systems. Thus, the EMB has the merit of shorter braking distance than that of conventional hydraulic brakes due to its better response time. At the beginning of EMB development, high-torque and high-power motors are required.

These requirements reveal some limits of the new system, which

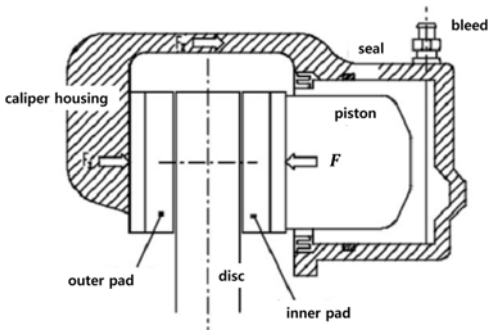

Fig. 1 Schematic diagram of a conventional hydraulic caliper

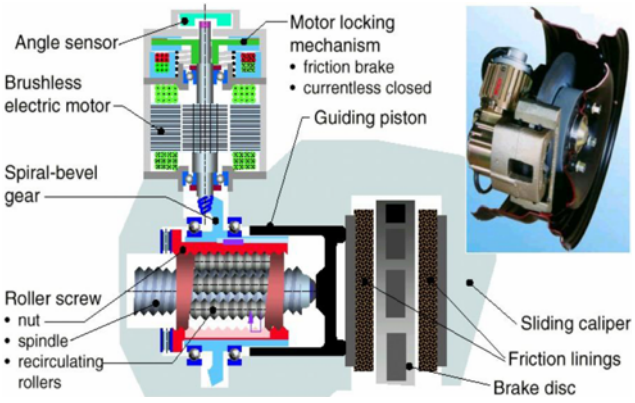

Fig. 2 Schematic diagram and prototype of electro mechanical brake[1]

will need big spaces and will impose high costs. For this reason, the electro wedge brake (EWB) is being launched with the self-reinforcement features of a wedge structure. The EWB can generate strong clamping forces using small size and low-torque motors with good braking efficiency and clamping efficiency.[2-10] In this paper, as a part of a high efficiency electro wedge brake, we describe a wedge structure that has a self-reinforcing effect; we also propose the proper actuating direction of the movable wedge for better braking efficiency. In section 2, we describe conventional brake systems such as those of hydraulic type, electro mechanical type, and electro wedge type. In section 3, we describe case studies of wedge actuating methods in order to select the most proper and efficient actuating method. In section 4, we describe the method of getting the higher braking efficiency and clamping efficiency regardless the variation of frictional coefficient with the estimation of frictional coefficient and the variable counter wedge structure. In section 5, we present the conclusions of this study.

2. Conventional Brake System

2.1 Hydraulic brake caliper

The braking process of a vehicle can be divided into the following two steps. In the first step, there is the rigid body behavior of the caliper. The caliper has a prismatic sliding motion before the contact between the pads and the disc. In the second step, there is the elastic body behavior of the caliper and the drive mechanisms with the pads.

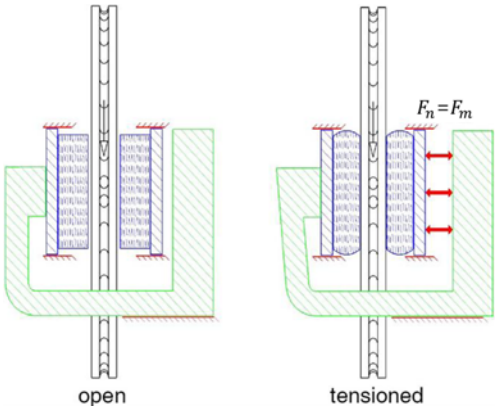

Fig. 3 Conceptual diagram and prototype of electro mechanical brake[2]

After the contact between the pad and the disc, the caliper undergoes elastic deformation until the required clamping force is generated.

Fig. 1 provides schematic diagrams of a conventional hydraulic brake caliper.[2] A hydraulic piston pushes an inner pad. Then, the inner pad moves toward the disc and generates clamping force after the contact between the inner pad and the disc. Then, the generated reaction force moves the caliper with the outer pad in the opposite direction of the motion of the inner pad. This mechanism induces clamping on two sides of the disc. Then, the rotating disc is decelerated. The braking force is equal to the clamping force multiplied by the frictional coefficient. This system uses hydraulic power.

2.2 Electro mechanical brake caliper

Fig. 2 provides a schematic diagram and a prototype of an electro mechanical brake that was presented by Bosch Co. Ltd. in 1997.[1] This mechanism has features that can substitute for those of a hydraulic brake system, such as a piston and cylinder connected to an electric motor with a reduction gear and a screw system. This system uses electric power, not hydraulic power. Fig. 3 shows a concept diagram of the direct clamping type system.[2] The conventional hydraulic caliper and the electro mechanical brake use the direct clamping method. In this method, the clamping force is induced by the actuating force only. Therefore, the electro mechanical brake must utilize the high power motor shown in the prototype shown in Fig. 2. Using this direct clamping method, we can obtain the braking efficiency shown in Eq. (1). Also, Eq. (2) shows the clamping efficiency. As is well known, the friction force is multiplication with both the normal force (the clamping force in the brake system) and the frictional coefficient. This relation is shown in Eq. (6).

$$C_b^* = \frac{F_b}{F_m} = \mu \tag{1}$$

$$C_n^* = \frac{F_n}{F_m} = 1 \tag{2}$$

Here, F_b means the braking resultant force; F_n is the clamping resultant force; F_m is the braking effort force, in other words the actuating force; μ is the frictional coefficient between the pad and the disc.

2.3 Electro wedge brake caliper

Fig. 4 provides a concept diagram of the electro wedge brake. This

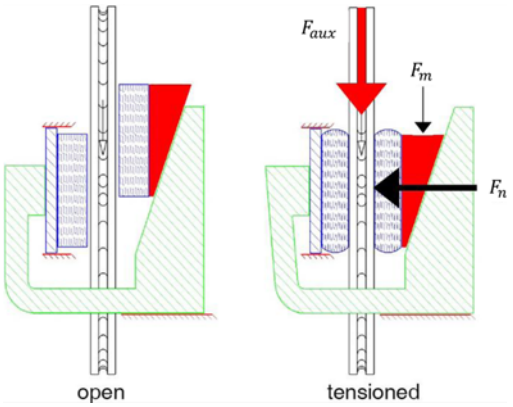

Fig. 4 Concept diagram of electro wedge brake[2]

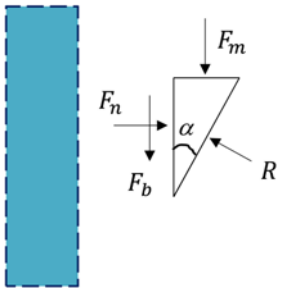

Fig. 5 Free-body diagram of movable wedge during clamping

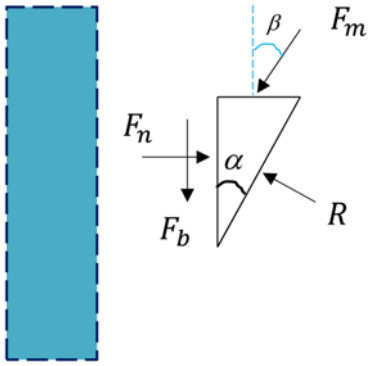

Fig. 6 Free-body diagram of movable wedge with the actuating direction

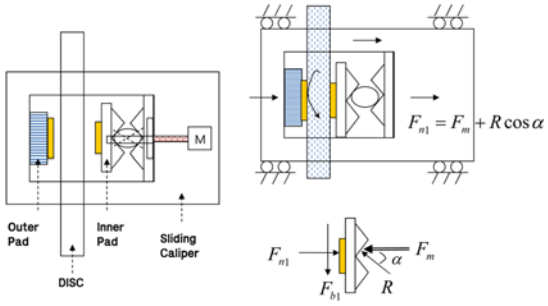

Fig. 7 Layout and free-body diagram of movable wedge of normal forcing method

mechanism is composed mainly of a movable wedge and a counter wedge. The actuating force F_m acts on the movable wedge. The movable wedge is pushed downward along the disc's rotational direction, as shown in Fig. 4. This mechanism leads to a process via which a small actuating force generates a large clamping force with the braking resultant force. This is a self-reinforcing effect. It is due to the frictional effect that arises as the inner pad moves along the disc; then, it seems that the inner pad obtains another actuating force beyond the original actuating force. For the self-reinforcing effect, the braking target, such as the disc, has kinetic energy. That is to say, a stationary disc does not lead to a wedge structure necessary to obtain the self-reinforcing effect. In the electro wedge brake caliper, we can obtain a braking efficiency C_b^* as shown in Eq. (3).

$$C_b^* = \frac{F_b}{F_m} = \frac{\mu}{\tan\alpha - \mu} \tag{3}$$

Here, α indicates the wedge inclinational angle. This equation is induced from a free-body diagram (Fig. 5) and from statics analysis (Eqs. (4)~(6)). In this paper, we assume that the tangential friction force of the reaction force on the wedge surface is small, due to the lubrication of plane contact surface or the line contact by using the roller disposed between movable wedge and counter wedge. If there is the plane contact without the lubrication between the movable wedge and counter wedge, then the frictional coefficient and the frictional force of the reaction force is not small and should take into account at the free body diagram.

$$\rightarrow \Sigma F = 0: \quad F_n - R\sin\alpha = 0 \tag{4}$$

$$\downarrow \Sigma F = 0: \quad F_m + F_b - R\sin\alpha = 0 \tag{5}$$

$$\text{Phenomenon of Friction: } F_b = \mu \times F_n \tag{6}$$

Here, R indicates the reaction force between the movable wedge and the counter wedge. In Eq. (3), we can get the important phenomenon that if we design the wedge inclinational angle α close to the frictional coefficient μ, then we can get a big braking force F_b with small actuating forces F_m. On the other hands, if tan (α) is lower than μ, then the movable wedge is pulled. It means that the actuating force has the negative value. Therefore the braking force is keeping the positive value.

Further, the additional design factor is the actuating direction on the movable wedge, as shown in Fig. 6. There are the normal forcing (β = 90 deg), tangential forcing (β = 0 deg) and inclinational forcing (0 deg < β < 90 deg) methods. If we select a proper actuating method, it will also contribute to the electro wedge brake system to yield more braking efficiency.

3. Case Studies of Wedge Actuating Methods

3.1 Case 1: normal forcing (β = 90 deg) method

Fig. 7 shows the layout and the free-body diagram of the movable wedge of the normal forcing case (β = 90 deg).

From the free-body diagram of the movable wedge (Fig. 7, right-bottom diagram) with statics analysis (Eqs. (7) and (8)), we can obtain the final braking efficiency (Eq. (9)) and clamping efficiency (Eq. (10)).

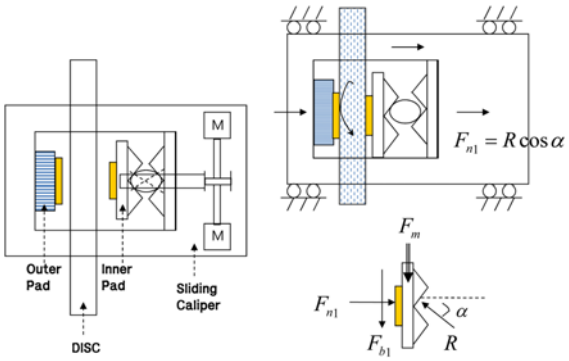

Fig. 8 Layout and free-body diagram of movable wedge of tangential forcing case

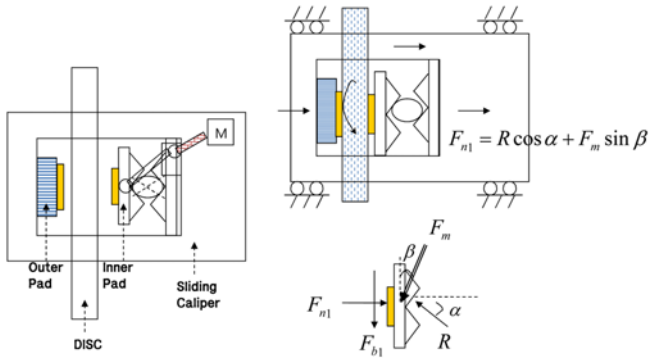

Fig. 9 Layout and free-body diagram of movable wedge of inclinational forcing case

In Eq. (9) compared with Eq. (3), there is an additional term in the numerator, tan α. This additional term leads to get less braking efficiency than Eq. (3). As is well-known, the frictional coefficient has a range from 0.3 to 0.6. Thus, if we design the wedge inclination angle as the averaged value of the frictional coefficient, like tan $\alpha = 0.45$ ($\alpha = 0.423$ rad = 24.24 deg), then the braking efficiency is less than Eq. (3).

$$F_{n1} = F_m + R\cos\alpha \tag{7}$$

$$F_{b1} = \mu F_{n1} = R\sin\alpha \tag{8}$$

$$C_b^* = \frac{F_{b1}}{F_m} = \frac{\mu}{\tan\alpha - \mu} \times \tan\alpha \tag{9}$$

$$C_n^* = \frac{F_{n1}}{F_m} = \frac{1}{\tan\alpha - \mu} \times \tan\alpha \tag{10}$$

3.2 Case 2: tangential forcing ($\beta = 0$ deg) method

Fig. 8 shows the layout and the free-body diagram of the movable wedge of the tangential forcing case ($\beta = 0$ deg). In this case, from the free-body diagram of the movable wedge (Fig. 8, right bottom diagram) with the statics analysis (Eqs. (11) and (12)), we can obtain the final braking efficiency (Eq. (13)) and clamping efficiency (Eq. (14)).

$$F_{n1} = R\cos\alpha \tag{11}$$

$$F_{b1} = \mu F_{n1} = R\sin\alpha - F_m \tag{12}$$

$$C_b^* = \frac{F_{b1}}{F_m} = \frac{\mu}{\tan\alpha - \mu} \tag{13}$$

$$C_n^* = \frac{F_{n1}}{F_m} = \frac{1}{\tan\alpha - \mu} \tag{14}$$

Eq. (13) is the same as Eq. (3). This result shows that the mechanism in Fig. 4 also has tangential forcing.

3.3 Case 3: inclinational forcing (0 deg < β < 90 deg) method

Fig. 9 shows the layout and the free-body diagram of the movable wedge of inclinational forcing case (0 deg < β < 90 deg). In this case, from the free-body diagram (Fig. 9, right bottom diagram) with statics analysis (Eqs. (15) and (16)), we can obtain the final braking efficiency (Eq. (17)) and clamping efficiency (Eq. (18)). Note that both the wedge inclinational angle α and the actuating angle β have the range of 0 deg < α, β < 90 deg.

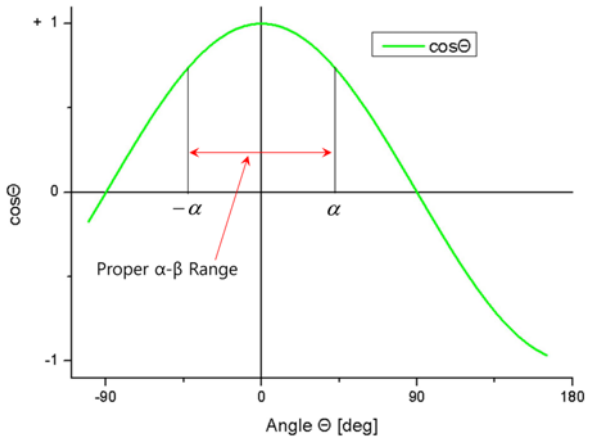

Fig. 10 Cosine diagram and the proper range of α–β

$$F_{n1} = R\cos\alpha + F_m \sin\beta \tag{15}$$

$$F_{b1} = \mu F_{n1} = R\sin\alpha - F_m \cos\beta \tag{16}$$

$$C_b^* = \frac{F_{b1}}{F_m} = \frac{\mu}{\tan\alpha - \mu} \times \frac{\cos(\alpha - \beta)}{\cos\alpha} \tag{17}$$

$$C_n^* = \frac{F_{n1}}{F_m} = \frac{1}{\tan\alpha - \mu} \times \frac{\cos(\alpha - \beta)}{\cos\alpha} \tag{18}$$

In Eq. (17), compared to Eq. (3), there is an additional term in the numerator, cos (α–β), and in the denominator, cos (α). These additional terms should have the proper range shown in Fig. 10. This range indicates that cos (α–β) is greater than cos (α).

As shown in Fig. 10, it is proper for the actuating angle β to select within the range of $-\alpha < \alpha - \beta < \alpha$. As a result, the actuating angle should have $0 < \beta < 2\alpha$ for greater braking efficiency than that of existing conventional electro wedge brakes. Fig. 11 shows the embodiment's example of inclinational forcing type EWB.[2]

3.4 Summary and comparison study

Table 1 provides a free-body diagram of the movable parts (wedge with pad) and the braking efficiency for each actuating method. Fig. 12 shows the comparison simulation results. This shows that the braking

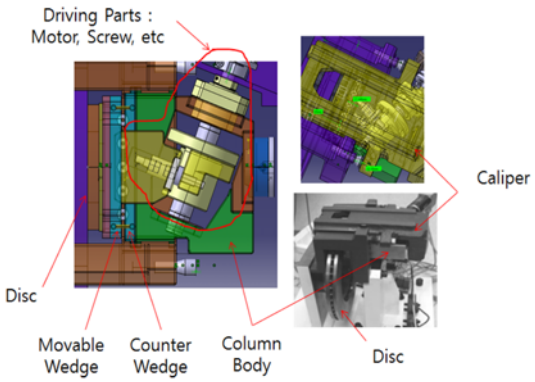

Fig. 11 Embodiment example of EWB; inclinational forcing type[2]

efficiency according to the variation of the frictional coefficient. This simulation has the same condition of α at 20.55 deg and β at 20 deg. Therefore, the asymptotic line is laid on μ as 0.375 = tan (20.55 deg), shown in Fig. 12. In Fig. 12, the left side of asymptotic line is push area which means driving parts push the movable wedge in clamping states with the deformation of mechanical structures, and the right side of asymptotic line is pull area which means driving parts push the movable wedge in clamping states with the deformation of mechanical structures.

As was afore-mentioned, the inclinational forcing case has the highest braking efficiency. So to speak, regarding to the design of the wedge inclinational angle α, upper-mentioned in section 2.3, it is suitable for the wedge inclinational angle α to select the nearby the frictional coefficient μ, then we can get a big braking force F_b with small actuating forces F_m. Further, regarding to the design of the actuating angle β, upper-mentioned in section 3.3, it is suitable for the actuating angle β to have the range of $0 < \beta < 2\alpha$, for greater braking efficiency than that of existing conventional electro wedge brakes.

On the other hand, there is a demerit to the inclinational forcing case. This occurs during reverse-driving braking of a vehicle. The braking efficiency during reverse driving for the inclinational forcing case is shown in Eq. (19).

Compared with Eq. (17), there is a difference in the numerator, cos (α+β). The numerator of cos (α+β) is always smaller than the denominator of cos (α). So, the braking efficiency during reverse driving for the inclination forcing case is lower than that for the tangential forcing case. However, the kinetic energy of reverse driving is lower than forward driving. Therefore, this demerit of inclinational forcing case is not significant.

$$C_b^* = \frac{F_b}{F_m} = \frac{\mu}{\tan\alpha - \mu} \times \frac{\cos(\alpha+\beta)}{\cos\alpha} \tag{19}$$

Until now, we assigned the frictional coefficient as the constant. However in the real world, the frictional coefficient is varied along the circumstance such as humidity, temperature, etc.

If the wedge angle is fixed, then the braking efficiency is lower than the initial designed value of braking efficiency. This shows at the left side of asymptotic line such as the braking efficiency of 8 at μ as 0.3 (the minimum frictional coefficient value), and the right side of asymptotic line such as the braking efficiency of 5 at μ as 0.6 (maximum frictional coefficient value) in Fig. 12.

Table 1 FBD and braking efficiency per case

Free body diagram of movable wedge	Braking Efficiency
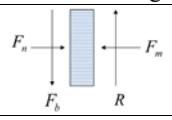	$C_b^* = \frac{F_b}{F_m} = \mu$
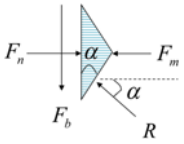	$C_b^* = \frac{F_b}{F_m} = \frac{\mu}{\tan\alpha - \mu} \times \tan\alpha$
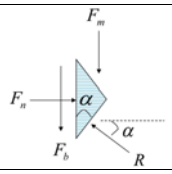	$C_b^* = \frac{F_b}{F_m} = \frac{\mu}{\tan\alpha - \mu}$
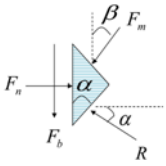	$C_b^* = \frac{F_b}{F_m} = \frac{\mu}{\tan\alpha - \mu} \times \frac{\cos(\alpha-\beta)}{\cos\alpha}$

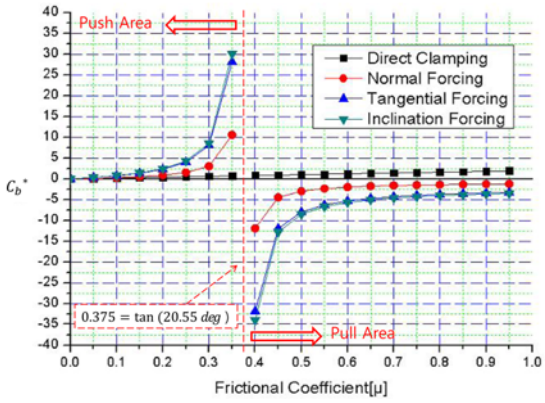

Fig. 12 Braking efficiency along with the variations of frictional coefficient per case

Therefore, in order to overcome this limit, in the next section we describe the method to keep the most braking efficiency and clamping efficiency without reference to the variations of frictional coefficient, with the estimation of frictional coefficient μ and the design of adaptive wedge angle α mechanism.

4. Variable Counter Wedge and Estimation of Frictional Coefficient

In this section, we describe the method of getting the higher braking efficiency regardless the variation of frictional coefficient. This method is composed with the estimation of frictional coefficient and variable counter wedge structure. For simple explanations, we select the tangential forcing structures. Fig. 13 shows the concept of driving structure of EMB and EWB with the resultant clamping force.

The estimation of frictional coefficient in EWB is derived from the

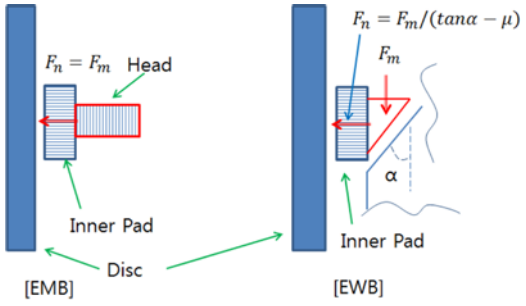

Fig. 13 Concept of driving structure of EMB and EWB with the resultant clamping force

relation of F_n and F_m shown in Fig. 13's right side. This relation is shown in Eq. (20).

$$F_n = \frac{F_m}{(\tan\alpha - \mu)} \tag{20}$$

The clamping force F_n can be measured by the load-cell in EWB, the actuating force F_m can be calculated by the driving mechanism from the motor torque, and the wedge angle α is decided in design steps. Then we can estimate the frictional coefficient μ only in EWB. This is shown in Eq. (21). Based on this idea, we describe the estimation of the fictional coefficient μ and variable counter wedge for the higher braking efficiency regardless the variation of frictional coefficient.

$$\alpha = \text{atan}\left(\mu + \frac{F_m}{F_n}\right) \tag{21}$$

On the other hands, in EMB, the estimation of frictional coefficient is impossible if the disc does not have the torque-meter attached along the disc shaft.

Fig. 14 shows the control loop of clamping force and counter wedge angle loop in EWB. The initial designed clamping efficiency C_n* which means the ratio of the clamping force F_n and the actuating force F_m is shown in Eq. (22).

$$C_n{}^*{}_{designed} = \frac{F_n}{F_m} = \frac{1}{\tan\alpha_0 - \mu_0} \tag{22}$$

Here α_0 means the initial designed counter wedge angle and μ_0 means the nominal frictional coefficient which is used to design the α_0.

In Fig. 14, the equation of frictional coefficient μ_{i_est} is derived from Eq. (20). This uses the actuating force F_{mi} on the movable wedge, the clamping force F_{ni} measured from the loadcell and measured the counter wedge angle α_i. Here i means the iterational number on the i th sampling. Eq. (23) shows the estimation of frictional coefficient μ_{i_est}.

$$\mu_{i\_est} = \tan\alpha_{i-1} - \frac{F_{mi}}{F_{ni}} \tag{23}$$

Based on this estimated frictional coefficient μ_{i_est}, we can get the command signal of counter wedge angle $\alpha_{i\_command}$ which is used to input command signal to the counter wedge control loop. Eq. (24) shows the command signal of counter wedge angle.

$$\alpha_{i\_command} = \text{atan}\left(\mu_{i\_est} + \frac{F_{mi}}{F_{ni}}\right) \tag{24}$$

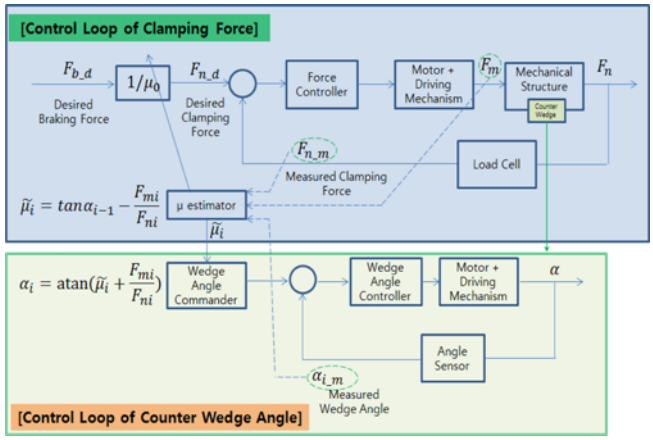

Fig. 14 Control loops for clamping and variable counter wedge angle

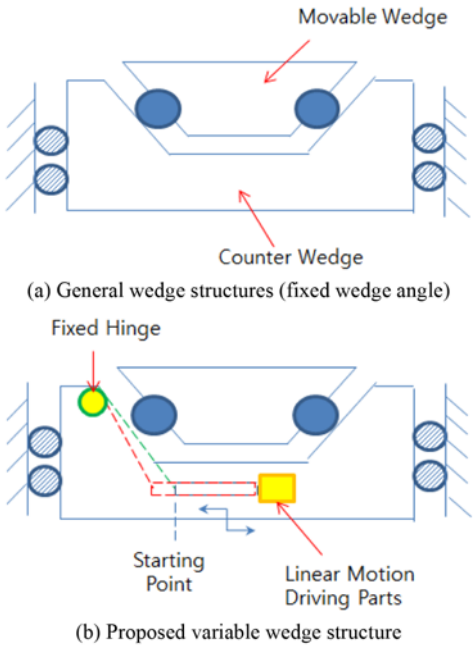

Fig. 15 Layout of variable wedge structure

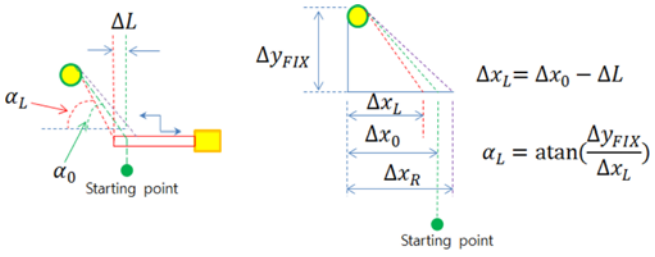

Fig. 16 Geometric analysis for extracting the command linear displacement of linear motion driving parts

Fig. 15 shows the general wedge structure (fixed wedge angle) and proposed variable wedge structure.

The movable wedge has the roller for reducing the loss of friction. Then, we dispose the fixed hinge and linear motion driving parts in the

counter wedge for the embodiment of variable wedge structure shown in Fig. 15(b).

Fig. 16 shows the geometric analysis for extracting the command linear displacement of linear motion driving parts in a given the command wedge angle shown in Eq. (24).

The starting point of the linear motion driving parts makes the initial wedge angle α_0. If the linear motion driving parts has the motion left directional displacement ΔL, then the wedge angle becomes α_L. From the geometric analysis, we can get the command linear displacement of linear motion driving parts in a given the command wedge angle. Eq. (25) shows this relation between the linear displacement of driving parts and the wedge angle.

$$\Delta L_{command} = \Delta x_0 - \Delta x_{L\_command} = \Delta x_0 - \frac{\Delta y_{FIX}}{\tan \alpha_{command}} \tag{25}$$

In this section, we described the method to keep the most braking efficiency and clamping efficiency without reference to the variations of frictional coefficient, with the estimation of frictional coefficient μ and the design of adaptive wedge angle α mechanism.

5. Conclusion

In this paper, we described the self-reinforce effect of the wedge mechanism in the braking system of vehicle. Further we investigated the actuating methods of movable wedge with the each braking efficiency. Through the analysis of four actuating cases, we revealed the proper actuating angle's range in the inclinational actuating method for getting more braking efficiency. As a result, regarding to the design of the wedge inclinational angle α, afore-mentioned in section 2.3, it is suitable for the wedge inclinational angle α to select the nearby the frictional coefficient μ, then we can get a big braking force F_b with small actuating forces F_m. Further, regarding to the design of the actuating angle β, afore-mentioned in section 3.3, it is suitable for the actuating angle β to have the range of $0 < \beta < 2\alpha$, for greater braking efficiency than that of existing conventional electro wedge brakes. Further we discussed the limit and this limit of significance in the inclinational actuating method.

On the other hands, we assigned the frictional coefficient as the constant by section 3 in this paper. However in the real world, the frictional coefficient is varied along the circumstance such as humidity, temperature, etc. If the wedge angle is fixed, then the braking efficiency is lower than the initial designed value of braking efficiency. Therefore we investigate the estimation of frictional coefficient μ and the design of adaptive wedge angle α mechanism for the most braking efficiency and clamping efficiency without reference to the variations of frictional coefficient.

ACKNOWLEDGEMENT

This work was supported by the DGIST R&D Program of the Ministry of Science, ICT and Technology of Korea (15-RS-03).

REFERENCES

1. DGIST, "Development of High Braking Efficiency Electro Mechanical Brake Technology," 2009.
2. Shin, D. H., Kwon, O. S., and Bae, J., "Study of EMB System using Wedge Structure," Transactions of the Korean Society of Automotive Engineers, Vol. 18, No. 3, pp. 8-18, 2010.
3. Shin, D. H., Park, T. S., Jin, S. H., Moon, J. I., and Yang, S. H., "Study of Mechanism for Wear Adjustment with Electro Wedge Brake," Key Engineering Materials, Vol. 625, pp. 712-716, 2015.
4. Shin, D. H., Kwon, O. S., Moon, J. I., and Yang S. H., "Cost-Effective Approaches of Circumferential Electro Wedge Brake for Reducing Unbalance-wears," Journal of Mechanics Engineering and Automation, Vol. 2, No. 4, pp. 208-212, 2012.
5. Shin, D. H. and An, J., "Study of Stiffness Design of Caliper for Reducing the Weight of an Electro Wedge Brake," Applied Mechanics and Materials, Vols. 138-139, pp. 159-162, 2012.
6. Hartmann, H., Schautt, M, Pascucci, A. and Gombert, B., "eBrake® - the Mechatronic Wedge Brake," SAE Technical Paper, Document ID: 2002-01-2582, 2002
7. Roberts, R., Schautt, M., Hartmann, H., and Gombert, B., "Modeling and Validation of the Mechatronic Wedge Brake," SAE Technical Paper, Document ID: 2003-01-3331, 2003.
8. Roberts, R., Gombert, B., Hartmann, H., Lange, D., and Schautt, M., "Testing the Mechatronic Wedge Brake," SAE Technical Paper, Document ID: 2004-01-2766, 2004.
9. Ho, L. M., Roberts, R., Hartmann, H., and Gombert, B., "The Electronic Wedge Brake-EWB," SAE Technical Paper, Document ID: 2006-01-3196, 2006.
10. Fox, J., Roberts, R., Baier-Welt, C., Ho, L. M., Lacraru, L., and Gombert, B., "Modeling and Control of a Single Motor Electronic Wedge Brake," SAE Technical Paper, Document ID: 2007-01-0866, 2007.